EFFECTS OF AXIAL AND CENTRIFUGAL FORCES ON THE STABILITY OF LIQUID BRIDGES

I. Martínez[1], J.M. Perales[2] & M. Gómez[2]

[1]E.T.S.I. Navales, Universidad Politécnica, 28040 Madrid, Spain
[2]Lamf-ETSIA, Universidad Politécnica, 28040 Madrid, Spain

ABSTRACT

Liquid bridges held by surface tension between two coaxial discs are of interest to fluid science in space and to the modelling of the very important crystal growth technology known as floating zone processing.

The equilibrium and stability equations for liquid bridges are well-known, but they are non-linear and it is difficult to guess real behaviour, such as the sensitivity of the shape to axial and rotational forces (measured by Bond and Weber numbers, respectively) or to the geometry of the solid supports that support the bridge.

This paper presents a parametric study by numerical methods of the different effects, and the analytical solutions at the bifurcation points in the stability diagrams.

These results will be of great help to plan future space experiments on liquid columns and floating zones in space, and in particular will show a method to easily measure very weak residual forces in microgravity platforms.

Keywords: capillarity, stability, microgravity, liquid bridge.

1. INTRODUCTION

The liquid bridge configuration is well known in microgravity research for its own merit as a simple and controllable setup for basic Fluid Science and for its direct application to the floating zone technique of crystal growth (Ref. 1).

Most of the past research on liquid bridge behaviour (and presumably most of the future work) has concentrated on the modelling of nearly cylindrical liquid bridges, because of the simplicity of the formulation of dynamic models (f.i. frequency responses (Refs. 2,3)), thermal models (f.i. Marangoni flows (Ref. 4)), electrical models (f.i. electric field intensity (Ref. 5)), etc., in the vicinity of a cylindrical bridge, that provides a simple rectangular domain in the meridian plane of this axisymmetric configuration.

For non-cylindrical liquid bridges, the static behaviour in absence of any other applied force but capillarity, allows for an analytical treatment in terms of elliptic integrals (Ref.6), but a residual gravity and/or rotation demands a numerical analysis.

The mathematical formulation of the equilibrium and stability of liquid bridges is well known (Ref. 7), and only their highly non-linear character that renders the guess difficult and the solution tedious, justify their detailed presentation. The knowledge gained in this exercise may be used to the following advantages:

- As check-points for more handy analytical models; to check their validity, to quantify their range of applicability and deviations, etc.
- As background stage for new effects here not considered; f.i., this work only takes into account axisymmetric deformations, and it is already known that some regions in the stability diagrams, here marked as stable (axisymmetrically), are indeed unstable to non-axisymmetric perturbations.
- As a guide to experiments with liquid bridges or floating zones, to take safe stable margins, to minimise or quantify the effect of sideby perturbations (as the unwanted residual acceleration and g-jitter in space platforms, or the shape deformation caused by the rotation imposed to uniformize the temperature field); in summary, to tune the sensibility of the liquid bridge to our advantage, minimising it if disturbing, and maximising it if so desired to amplify its effect.

2. FORMULATION

Axisymmetric equilibrium shapes of liquid bridges anchored to the sharp edges of two solid supports are characterised by their meridian curve $R = R(z)$, Fig. 1, which is to be found for the prescribed geometry and stimuli; namely: the radii of the supports, R_1 (assumed to be the smaller) and R_2, their separation, L, the volume of liquid in between, V, an axial

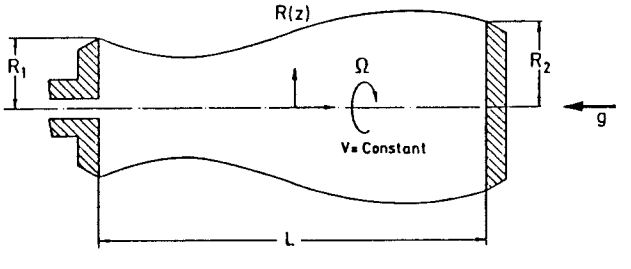

Fig. 1. Geometry and coordinate system for the liquid bridge problem.

Proceedings VIIIth European Symposium on Materials and Fluid Sciences in Microgravity, Brussels, Belgium, 12 - 16 April 1992, ESA SP-333 (August 1992)

constant acceleration, g (positive or negative), and a centrifugal force due to a solid-body rotation rate, Ω. In terms of a nondimensional set of parameters, the meridian curve can be written as:

$$R = R(z,L_r,V_r,H,Bo,We) \tag{1}$$

where $R = R/R_o$, $z = z/R_o$, $H = (R_2-R_1)/(2R_o)$, $L_r = L/(2\pi R_o)$, $V_r = V/(\pi R_o^2 L)$, $Bo = \Delta\rho g R_o^2/\sigma$, $We = \Delta\rho\Omega^2 R_o^3/\sigma$, $\Delta\rho$ is the density difference between the working liquid of the bridge and the surrounding atmosphere, σ their interfacial tension, and $R_o = (R_1+R_2)/2$. Bold and light characters above represent dimensional and non-dimensional variables, respectively.

The equilibrium shape $R(z)$ must verify the Young-Laplace capillarity equation:

$$C(z) - Bo\cdot z + \frac{We}{2}R^2(z) + P = 0 \tag{2}$$

where $C(z)$ is the local mean curvature at a point in the surface:

$$C(z) = \frac{R_{zz}}{\left(1+R_z^2\right)^{3/2}} - \frac{1}{R\left(1+R_z^2\right)^{1/2}} \tag{3}$$

$R_z = dR/dz$, $R_{zz} = d^2R/dz^2$, and P is a constant in Eq. 2 that corresponds to the non-dimensional gauge pressure at $z = 0$. The meridian extends from $z = -\pi L_r$ to $z = \pi L_r$, and must be anchored to the disc edge, i.e.

$$\begin{aligned} R(-\pi L_r) &= 1 - H \\ R(\pi L_r) &= 1 + H \end{aligned} \tag{4}$$

and must also preserve the volume:

$$V_r = \frac{1}{2\pi L_r}\int_{-\pi L_r}^{\pi L_r} R^2(z)dz \tag{5}$$

Let $T=R_z(-\pi L_r)$ be the initial slope of the meridian shape. The equilibrium problem on (L_r,V_r,H,Bo,We) is solved by transforming the boundary-value problem defined by Eqs. 1-5 to an initial-value problem on (L_r,V_r,H,Bo,We,T,P) that we solve numerically by the shooting method, and thence by finding the appropriate (T,P) for the given (H,V_r) using a Newton-Raphson procedure. The stability problem is solved by finding the singular points of the (T,P)-to-(H,V_r) transformation.

2.1. A shot shape

The following initial-value problem is numerically solved:

$$\left.\begin{aligned} A &= \left(1+R_z^2\right)^{1/2} \\ \frac{dR}{dz} &= R_z \\ \frac{dR_z}{dz} &= A^3\left(Bo\cdot z - \frac{We}{2}R^2 - P + \frac{1}{RA}\right) \\ \frac{dV_r}{dz} &= \frac{R^2}{2\pi L_r} \end{aligned}\right\} \quad \text{for} \quad z > -\pi L_r \tag{6}$$

with the initial values at $z = -\pi L_r$:

$$\left.\begin{aligned} R &= 1-H \\ R_z &= T \\ V_r &= 0 \end{aligned}\right\} \quad \text{at} \quad z = -\pi L_r \tag{7}$$

advancing with a constant step $h = 2\pi L_r/N$ (with N a chosen integer number) using a 4th-order Runge-Kutta algorithm, until the end value $z = \pi L_r$, where one gets two target parameters:

$$\left.\begin{aligned} H^+ &= R-1 \\ V_r^+ &= V_r \end{aligned}\right\} \quad \text{at} \quad z = \pi L_r \tag{8}$$

that depend on the parameter set (T,P,L_r,H,Bo,We,N), and that in general will differ from the desired end-values H and V_r. The effect of N on the end-result (H^+,V_r^+) is usually negligible for $N>20$, as shown below in the stability analysis.

Moreover, the Jacobian, J, of the transformation (T,P)-to-(H,V_r):

$$J = \begin{vmatrix} \frac{\partial H}{\partial P} & \frac{\partial H}{\partial T} \\ \frac{\partial V_r}{\partial P} & \frac{\partial V_r}{\partial T} \end{vmatrix} \tag{9}$$

is evaluated numerically with an increment in the parameters $\Delta T = \Delta P = \delta$ (typically $\delta = 10^{-6}$).

In summary, from a given list of input parameters $(L_r,V_r,H,Bo,We,T,P,N,\delta)$, the following list of output parameters is obtained $(R(z),V_r^+,H^+,J,\varepsilon_{equi})$, where a distance from goal to guess ε_{equi} is defined as:

$$\varepsilon_{equi} = |H^+-H| + |V_r^+-V_r| \tag{10}$$

2.2. The equilibrium shape

The solution of the original problem (L_r,V_r,H,Bo,We) is given by the solution of the non-linear system:

$$\begin{aligned} H &= H^+(P,T;L_r,V_r,H,Bo,We) \\ V_r &= V_r^+(P,T;L_r,V_r,H,Bo,We) \end{aligned} \tag{11}$$

A Newton-Raphson algorithm is used to find the correct input (T,P) to the initial-value shooting, within a given accuracy $\varepsilon_{equi} = |H^+-H| + |V_r^+-V_r|$, typically $\varepsilon_{equi} < 10^{-5}$. In summary, from a given list of input parameters $(L_r,V_r,H,Bo,We,T,P,N,\delta,\varepsilon_{equi})$, the following list of output parameters is obtained $(R(z),T,P,J)$, that is, the equilibrium shape $R(z)$, the two correct initial values (T,P) that produced it using the shooting algorithm and the Jacobian J at this point in the (T,P)-to-(H,V_r) transformation.

The above scheme to compute equilibrium shapes may look straightforward, but the tricky point is that the Newton-

Raphson algorithm only works if the initial guess is sufficiently close to the correct one, which of course is unknown. Thus, how to compute $R(z)$ for $L_r = 0.7$, $V_r = 0.8$, $H = 0.1$, $Bo = 0.05$ and $We = 0.1$, for instance?

Our approach is as follows. We always start solving for the trivial set of parameters $(L_r,V_r,H,Bo,We) = (L_r,1,0,0,0)$ that represent a cylindrical liquid bridge in absence of force fields, and start the Newton-Raphson search by shooting with $P = 1$ and $T = 0$, what of course gives the exact shape, $R(z) = 1$, right away. Thence, we compute nearby equilibrium shapes that differ from each other in the small amount:

$$\Delta L_r = 0, \Delta V_r = \frac{V_r - 1}{M}, \Delta H = \frac{H}{M}, \Delta Bo = \frac{Bo}{M}, \Delta We = \frac{We}{M} \quad (12)$$

where the integer M is chosen automatically in order to give the larger increment in Eq. 12 smaller than 10^{-2}, that happens to be good enough in our case, resulting in a value of $M = 4$ to $M = 20$, according to the cases (it might be set constant, equal to the larger value, but would waste computing time; by the way, it takes some seconds or up to a few tens of seconds in a HP-300 workstation to compute an equilibrium shape, as the one cited above).

2.3. The stability limits

We compute stability limits for the equilibrium shapes of liquid bridges by selecting an initial stable equilibrium shape (computed with the procedure explained above) and selecting an increment, d, and a running parameter that may be the set $(d,0,0,0,0)$, or $(0,d,0,0,0)$, or $(0,0,d,0,0)$, or $(0,0,0,d,0)$, or $(0,0,0,0,d)$, or any combination of them, as $(d,-dV_r/L_r,0,0,0)$ when a liquid bridge stretching at constant liquid volume is desired (remember that V_r is the ratio of real liquid volume to the so-called cylindrical volume $2\pi^2 L_r$).

The increment, d, in the running parameter is initially set to a large value, typicaly $d = 10^{-2}$ or $d = -10^{-2}$ as desired, and an additional variable, I, the maximum number of trials allowed for the Newton-Raphson search, is set, typically to a value $I = 20$. A shape-sequence routine then produces a series of equilibrium shapes that differ little from their predecessors and thus the Newton-Raphson search is very quick, since the former (T,P) values are used to start the search. Meanwhile, the Jacobian at each step is also computed, and the stability limit is found when the Jacobian becomes zero, a point that, of course, is not at reach because it is a singular point in the Newton-Raphson algorithm, although this problem is circumvented in the following manner.

Figure 2 shows an example of the evolution of the parameters during a shape sequence in which the Bond number, Bo, is increased (decreased) at constant geometry (H,L_r), volume, V_r, and Weber number, We. In Fig. 2a the natural plot versus the running parameter Bo is presented, and in Fig. 2b the same information is presented versus the Jacobian J.

The shape-sequence routine produces shapes that differ in $|d| = 10^{-2}$ in the running parameter, until the stable limit happens to be surpassed and the Newton-Raphson search fails; thence the value of $|d|$ is reduced to 1/3 of its former value and the last stable point is regained to start a finner advancing pace until the stable limit is surpassed again, repeating the partition until a desired tolerance, t, in the limiting value of the running parameter (typically $t \approx 10^{-4}$) is reached. At that point, the following extrapolation is applied (see an example in Fig. 2b): the limiting value of the running parameter is set to the vertex of a parabollae symmetric to $J = 0$ and fitted to the last 2 points (f.i. the last two 'x' points near $J = 0$ in Fig. 2b); the limiting value of the internal parameters P and T is found by parabollic extrapolation from the last two points near $J = 0$ up to $J = 0$. Thence, a last shot with these (P,T) values is run to produce new values H^{++}, V_r^{++} and J. In summary, from a given list of input parameters $(L_r,V_r,H,Bo,We,T,P,N,\delta,\varepsilon_{equi},t)$, the following list of output parameters is obtained $(R(z),T,P,J,L_r^{++},V_r^{++},H^{++},Bo^{++},We^{++})$. A measure of the departure from the exact stability limit is given by the distance ε_{stab} defined by:

$$\varepsilon_{stab} = |J| + |H^{++} - H| + |V_r^{++} - V_r| \quad (13)$$

where H and V_r are the original constraints that were imposed

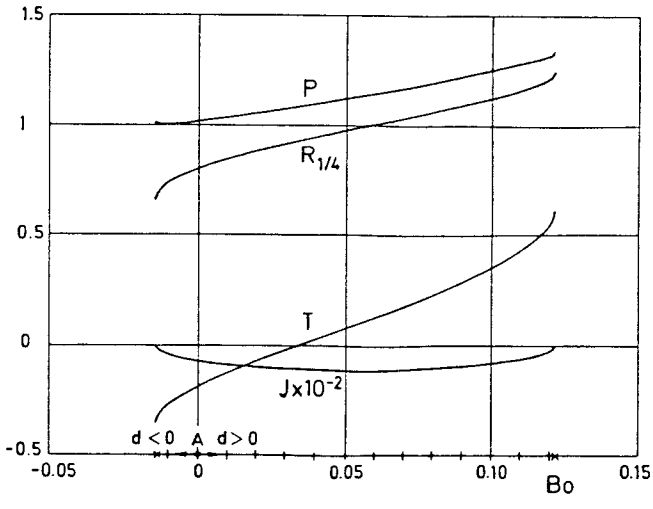

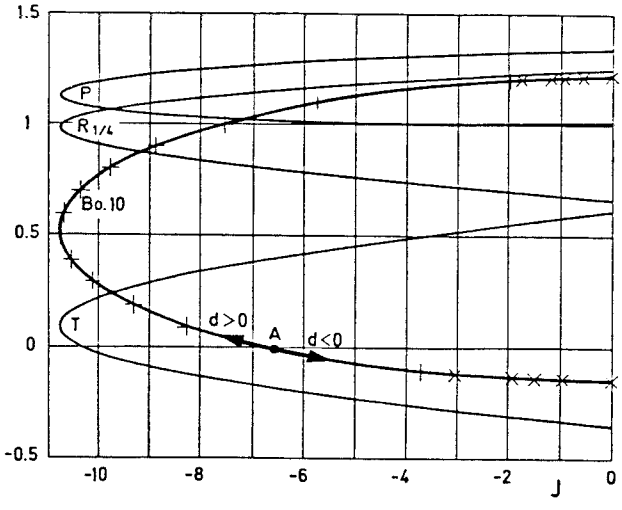

Fig. 2. Example of a sequence of equilibrium shapes starting from the set ($L_r = 0.8$, $V_r = 1$, $H = 0.1$, $Bo = 0$, $We = 0$), point A, and increasing the Bond number, Bo, with a step $d = 0.01$, or decreasing it with $d = -0.01$ (points marked with '+' in both cases), until the stability limit is coarsely found, decreasing the step d as shown in the points marked 'x' to find the limit more accurately. The two internal parameters P and T, and a characteristic shape point $R_{1/4}$ are plotted: a) versus the Bond number, Bo, b) versus the Jacobian, J.

to find the stability limit (obviously, for the running parameter there is no initial information to compare with, its constraint being translated to the zeroing of the Jacobian, J).

For the example in Fig. 2, where the limiting Bond number Bo is to be found for $L_r = 0.8$, $V_r = 1$, $H = 0.1$ and $We = 0$, Eq. 13 gives:

$$\varepsilon_{stab} = \left|-1.3\times10^{-2}\right| + |0.101 - 0.1| + |1.001 - 1| = 1.5\times10^{-2}$$

As said before, it is important to verify that the effect of the artificially introduced parameters in the numerical computation are negligible. Typically $N = 20$ for $L_r = 0{,}6$, although a larger value is needed for $L_r < 0{,}6$, as shown in Fig. 3, where the effect of N in a given result is depicted.

3. RESULTS

The approach explained above can be used to produce the following set of diagrams that show the static behaviour of liquid bridges:

1. Equilibrium shapes, up to the limit stable shape, as shown in Fig. 4 for $L_r = 0.8$ (it should be noted that the limit for $V_r - 1 = H = Bo = We = 0$ is $L_r = 1$, and that the typical limits exercised aboard Spacelab are near $L_r = 0.9$ (Ref. 8)). Figure 4a shows the trivial cylindrical shape for $(L_r, V_r, H, Bo, We) = (0.8, 1, 0, 0, 0)$ and the two limiting equilibrium shapes corresponding to maximum and minimum Bond number that for $H = 0$ happen to be equal in magnitude, $Bo_{limit} = \pm 0.070$. Figure 4b shows the non-trivial shape for $(L_r, V_r, H, Bo, We) = (0.8, 1, 0.1, 0, 0)$ and the two limiting equilibrium shapes corresponding to maximum and minimum Bond number that now are of different magnitude: $Bo_{max} = 0.122$ and $Bo_{min} = -0.014$. Only limiting equilibrium shapes are plot on Figs. 4c to f, to show the effect of changing H from 0 to 0.1 (left and right), of changing Bo from 0 to 0.05 (middle and bottom),

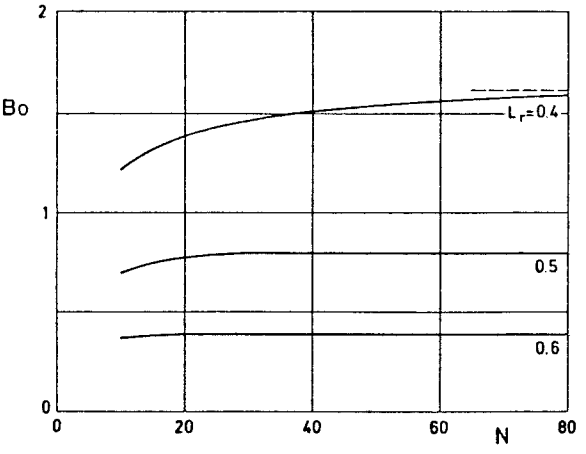

Fig. 3. Effect of the number of points, N, used in the Runge-Kutta routine that integrates the Young-Laplace equation, in the computation of the maximum Bond number, Bo, that a liquid bridge with $V_r = 1$, $H = 0$, and $We = 0$ can withstand, for three different slendernesses, L_r.

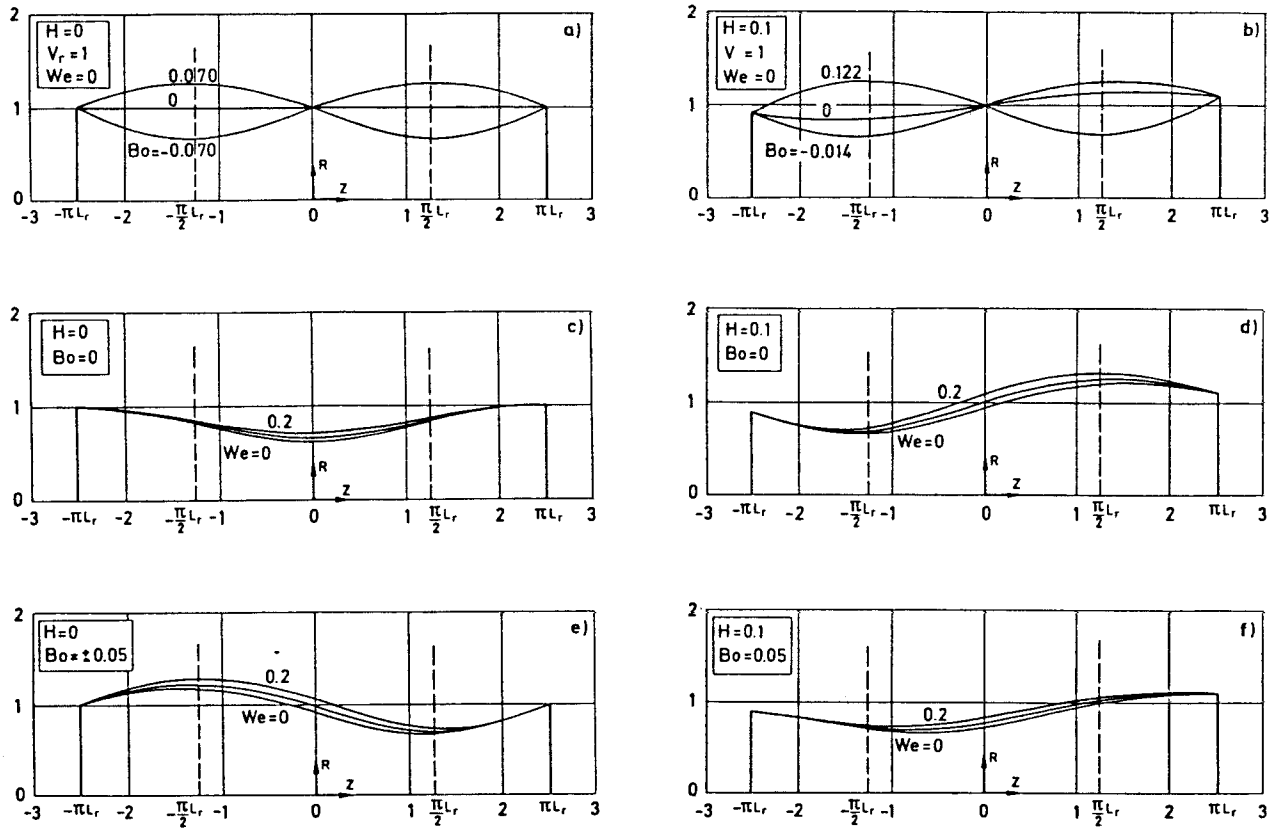

Fig. 4. Diagram of equilibrium shapes and their stability limits for $L_r = 0.8$ and several values of V_r, H, Bo and We.

and of changing the Weber number We (only the first three cases are shown in each picture). The volume of the limit shapes will not be cylindrical in general.

2. Deformation diagrams. We call deformation diagram a plot of a representative point of the equilibrium shape (that we choose coincident with the radius at a quarter of the liquid bridge length $z=\pi L_r/2$) as a function of one of the parameters in the set (L_r,V_r,H,Bo,We). Figure 5 gives several examples of these deformations diagrams.

3. Stability diagrams, where no information about shapes is retained and only the relation between the limiting values of the parameter set (L_r,V_r,H,Bo,We) is represented, as in Fig. 6.

4. ANALYTICAL APPROXIMATIONS TO THE STABILITY LIMITS

The intrinsic difficulty in numerically finding the solution of the problem given by Eqs. 1-5 can be circumvented by analytical approximations in the vicinity of some special configurations.

In the following expressions deduced from the results of Vega & Perales (Ref. 9) are given, the results being in agreement with numerical results in the region considered.

In that paper the configurations considered are close to the perfect cylinder which loses its stability by cnetrifugation, i.e. a neighbourhood of $(L_r,V_r,H,Bo,We) = (L_r,1,0,0,1/L_r^2-1)$ is considered.

To follow the standard Lyapunov-Schmidt method a new parameter, ε, measuring the projection of the departure of the equilibrium shape from the cylinder onto the non-trivial solution of the linear stability problem, is introduced.

Two different, but equivalent, approximations can be done:

A: If L_r is considered to be fixed then We should be closed to the value:

$$We_o(L_r)=\frac{1}{L_r^2}-1 \tag{14}$$

In this case, ε is deduced after the bifurcation equation, which reads:

$$-\varepsilon(We-We_o)+g_{20}(L_r)\varepsilon^3+\frac{2Bo}{\sqrt{1+We_o}}+0(\varepsilon^4)=0 \tag{15}$$

This equation has either 3 solutions in ε if $We < We_c$ (the stable one and two unstable) or only one if $We > We_c$. The function $g_{20}(L_r)$ coincides with equation (14) of Ref. 9:

$$g_{20}=-\frac{3\left(1+We_o+\frac{We_o^2}{2}+\frac{We_o^3}{4}\right)}{2(1+We_o)} \tag{16}$$

The equilibrium shape is given by:

$$R(z)=1+\varepsilon\sin\frac{z}{L_r}+\frac{\varepsilon^2}{4}\left[-\frac{We_o\cos\frac{z}{L_r}}{1+We_o}-1+\frac{\cos\frac{2z}{L_r}}{1+We_o}\right]+0(\varepsilon^3) \tag{17}$$

B: If We is considered to be fixed, L_r should be closed to:

$$L_{r_o}(We)=\frac{1}{\sqrt{1+We}} \tag{18}$$

and the bifurcation equation now reads:

$$-2\varepsilon\left[\frac{L_r}{L_{r_o}}-1\right](1+We)+g_{20}(We)\varepsilon^3+\frac{2Bo}{\sqrt{1+We}}+0(\varepsilon^4)=0 \tag{19}$$

where $g_{20}(We)$ is computed by Eq. 16 changing We_o by We, and the equilibrium shape is given by Eq. 17 changing We_o by We and L_r by L_{r_o}.

$$R(z)=1-\varepsilon\sin\frac{z}{L_{r_o}}+\frac{\varepsilon^2}{4}\left[-\frac{We\cos\frac{z}{L_{r_o}}}{1+We}-1+\frac{\cos\frac{2z}{L_{r_o}}}{1+We}\right] \tag{20}$$

From the above expressions it can be deduced the deformation at any point and, particularly, at $z = 1/4$. For case A:

$$R_{1/4}(L_r,Bo,We)=1-\varepsilon-\frac{\varepsilon^2}{4}\frac{2+We_o}{1+We_o} \tag{21}$$

where ε is deduced after Eq. 15. For case B it is the same but changing in (21) We_o by We and deducing e after Eq. (19).

The limit point of the curves represented in Fig. 5 (the stability limit) can be deduced from Eq. 20 by substituting for ε the value where $dWe/d\varepsilon = 0$, the result being

$$\varepsilon_{limit}=\varepsilon_{limit}(Bo,We)=\left(\frac{Bo}{g_{20}(L_r)\sqrt{1+We_o}}\right)^{1/3}=\sqrt{\frac{We-We_o}{3g_{20}(L_r)}} \tag{22}$$

or

$$\varepsilon_{limit}=\varepsilon_{limit}(Bo,We)=\left(\frac{Bo}{g_{20}(We)\sqrt{1+We}}\right)^{1/3}=\sqrt{\frac{2(1+We)(L_r/L_{r_o})}{3g_{20}(We)}} \tag{23}$$

The stability limits presented in Fig. 6 can be obtained by substituting Eqs. 22 and 23 in Eqs. 15 and 19, yielding:

$$We_{max}(L_r,Bo)=We_o+3\left(\frac{g_{20}(L_r)Bo^2}{1+We_o(L_r)}\right)^{1/3} \tag{24}$$

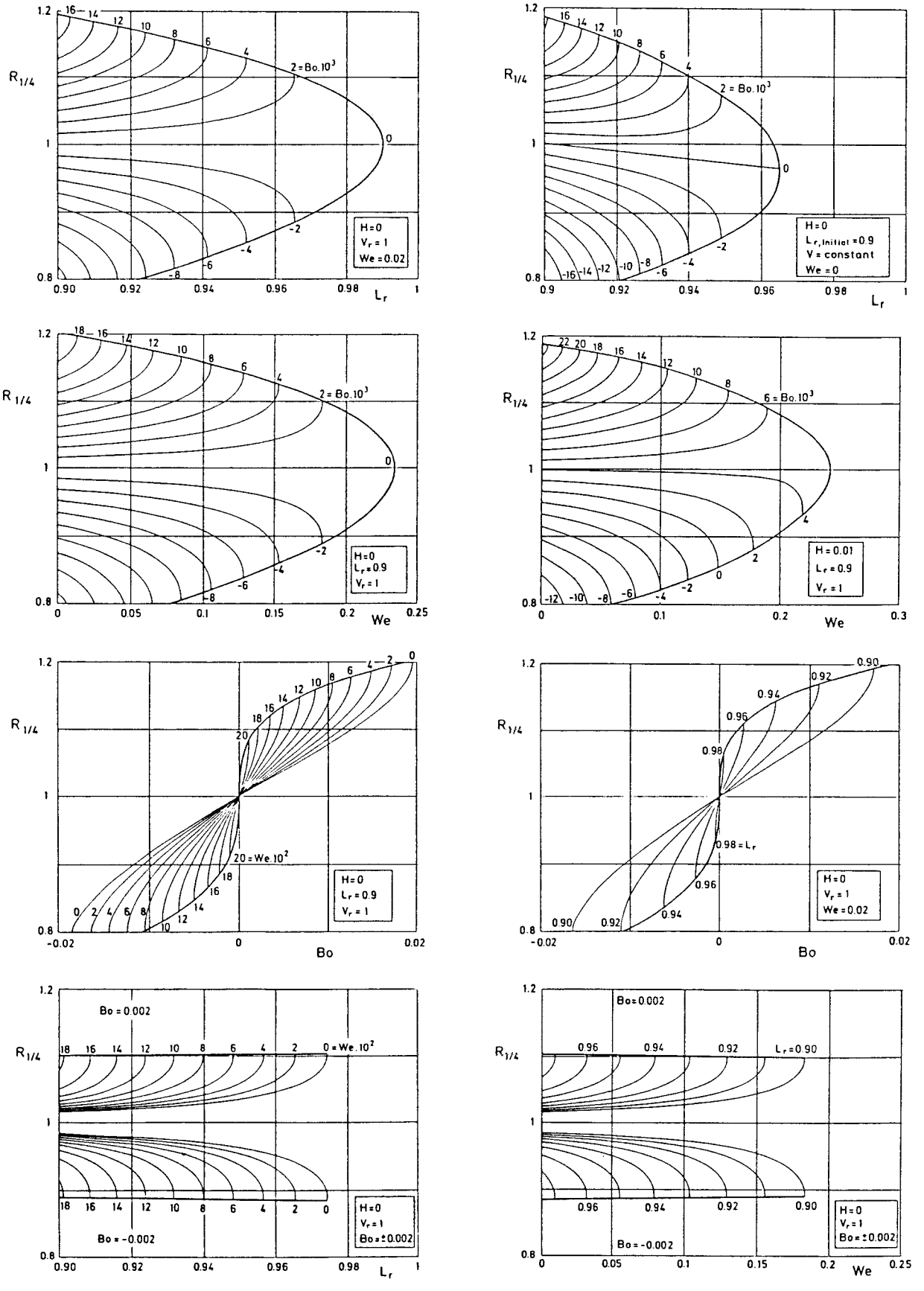

Fig. 5. Several deformation diagrams for liquid bridges. $R_{1/4}$ is the radius at a quarter of the bridge length.

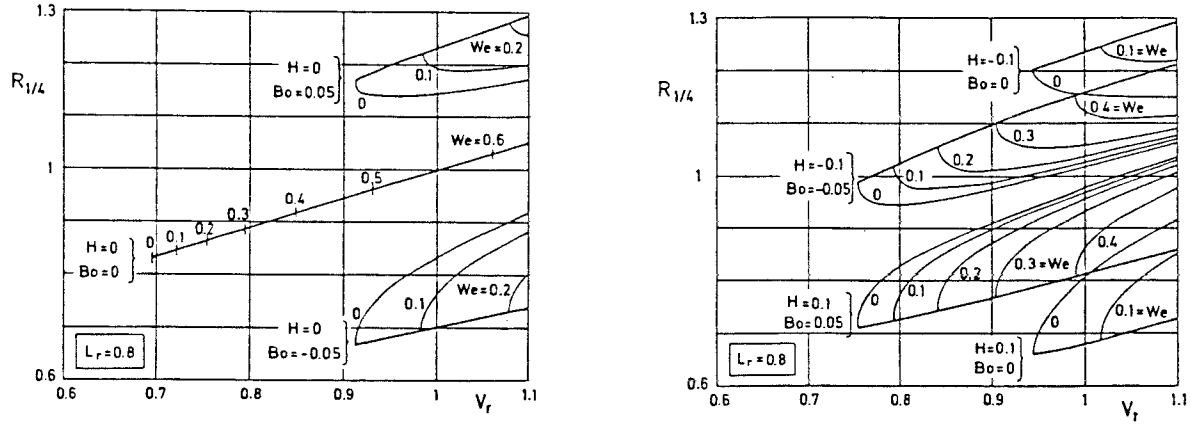

Fig. 5 (cont.). Several deformation diagrams for liquid bridges. $R_{1/4}$ is the radius at a quarter of the bridge length.

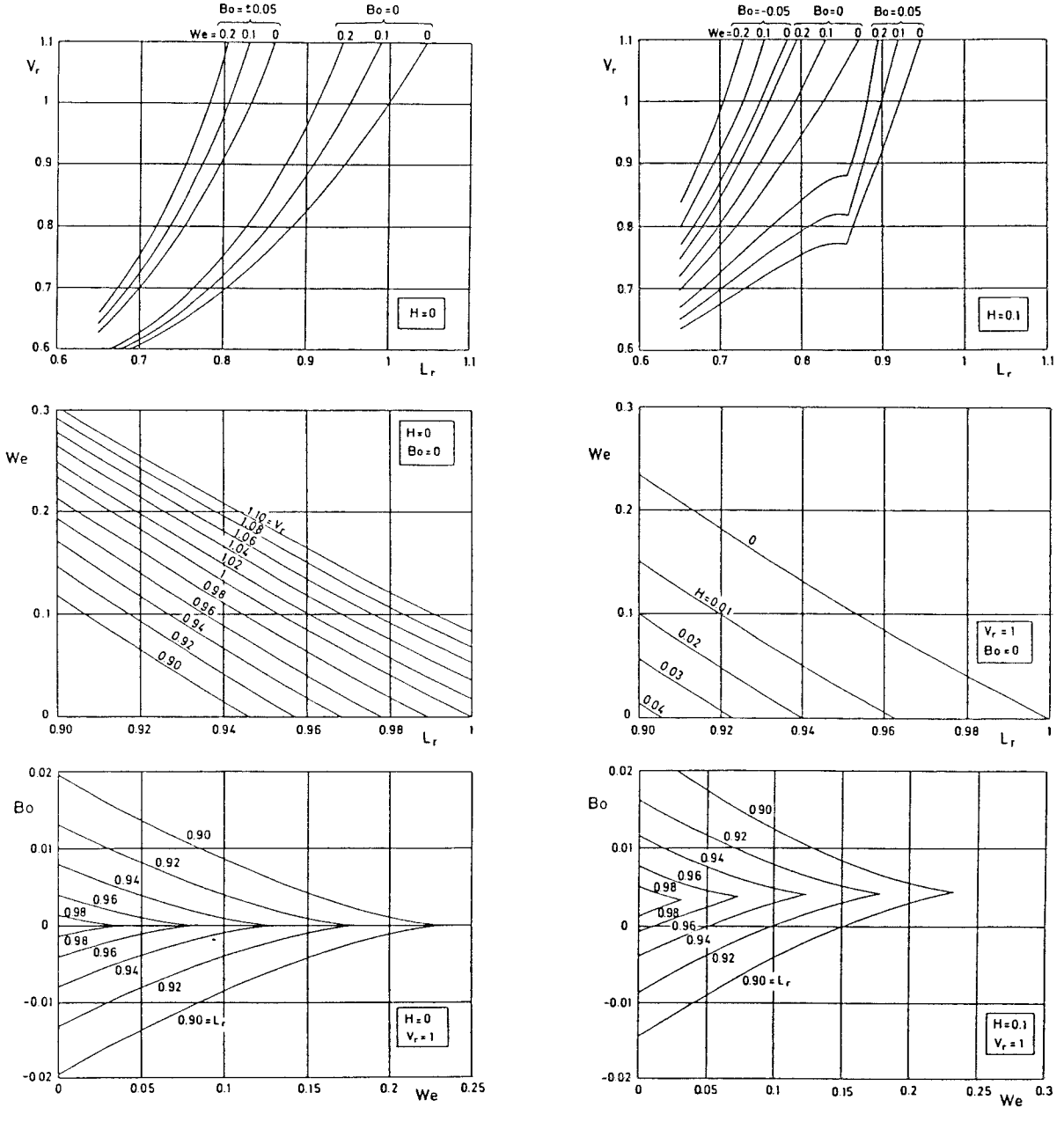

Fig. 6. Several stability diagrams for liquid bridges.

$$Bo_{\max}(L_r, We) = \sqrt{\frac{1+We_o}{g_{20}(L_r)}\left(\frac{We-We_o}{3}\right)^3} \qquad (25)$$

$$L_{r\max}(Bo, We) = \frac{1}{\sqrt{1+We}}\left[1+\frac{3}{2}\frac{g_{20}^{1/3}(We)}{(1+We)^{5/3}}Bo^{2/3}\right] \qquad (26)$$

$$Bo_{\max}(L_r, We) = \left[\frac{2(1+We)^{5/3}}{3g_{20}^{1/3}(We)}(L_r\sqrt{1+We}-1)\right]^{3/2} \qquad (27)$$

5. CONCLUSIONS

The well-known shooting method to numerically compute equilibrium shapes of liquid bridges, and their stability limits, is applied here to a five parameter case, when different disc sizes (measured by H), bridge lengths (L_r), liquid volumes (V_r), residual axial acceleration (Bo) and solid-body centrifugation (We) are contemplated.

The bundle of diagrams here presented give an idea of the complexities of such a multi-parametric analysis, and may help in further research to delimitate other forms of instability (f.i. the skipping rope on centrifugation) not considered here.

The numerical results have been used to check the validity of several analytical asymptotic expressions, with perfect agreement over the range of interest here (long liquid bridges), but these models only take into consideration the subset (L_r,V_r=1,H=0,Bo,We) of the five parameter family.

Further work has been initiated along the two open lines described above: non cylindrical volume and unequal end discs.

ACKNOWLEDGEMENTS

This work has been sponsored by the Spanish Comisión Interministerial de Ciencia y Tecnología (CICYT) and is part of a more general endeavour for the study of fluid physics and materials processing under microgravity (Project No. ESP88-0359).

REFERENCES

1.- Martínez I 1992, Fluid Science Requirements for Columbus, *Space Technol.*, 12, 135-144.

2.- Sanz A 1985, The influence of the outer bath in the dynamics of axisymmetric liquid bridges, *J. Fluid Mech.*, 156, 101-140.

3.- Sanz A & López–Díez J 1989, Non-axisymmetric oscillations of liquid bridges, *J. Fluid Mech.*, 205, 503-521.

4.- López J 1991, Low-Marangoni low-Reynolds numbers capillary flow inside a slender liquid bridge, *Microgravity Sci. Technol.*, 3, 221-230.

5.- González H & al 1989, Stabilization of dielectric liquid bridges by electric fields in the absence of gravity, *J. Fluid Mech.*, 206, 545-561.

6.- Martínez I & Perales J M 1986, Liquid bridge stability data, *Journal of Crystal Growth*, 78, 369-378.

7.- Myshkis A D & al 1987, *Low-gravity fluid mechanics*, Springer Verlag, Berlin, 580 p.

8.- Martínez I & Sanz A 1990, Experiments with long liquid columns under microgravity, *Proc. VIIth European Symposium on Materials and Fluid Sciences in Microgravity*, ESA SP-295, 413-419.

9.- Vega J M & Perales J M 1983, Almost cylindrical isorotating liquid bridges for small Bond numbers, *Proc. IVth European Symposium on Materials Sciences in Microgravity*, ESA SP-191, 247-252.